Planetary and Space Science 59 (2011) 1960–1967

Contents lists available at ScienceDirect

Planetary and Space Science

journal homepage: www.elsevier.com/locate/pss

Mercury crater statistics from MESSENGER flybys: Implications for stratigraphy and resurfacing history

Robert G. Strom [a,*], Maria E. Banks [b], Clark R. Chapman [c], Caleb I. Fassett [d], Jeffrey A. Forde [e], James W. Head III [d], William J. Merline [c], Louise M. Prockter [f], Sean C. Solomon [g]

[a] Lunar and Planetary Laboratory, University of Arizona, Tucson, AZ 85721, USA
[b] Center for Earth and Planetary Studies, Smithsonian Institution, Washington, DC 20560, USA
[c] Southwest Research Institute, 1050 Walnut Street, Boulder, CO 80302, USA
[d] Department of Geological Sciences, Brown University, Providence, RI 02912, USA
[e] Microsoft Corporation, One Microsoft Way, Redmond, WA 98052, USA
[f] Johns Hopkins University Applied Physics Laboratory, Laurel, MD 20723, USA
[g] Department of Terrestrial Magnetism, Carnegie Institution of Washington, Washington, DC 20015, USA

ARTICLE INFO

Article history:
Received 21 July 2010
Received in revised form
3 March 2011
Accepted 25 March 2011
Available online 30 April 2011

Keywords:
Mercury
Cratering
Volcanism
MESSENGER

ABSTRACT

The primary crater population on Mercury has been modified by volcanism and secondary craters. Two phases of volcanism are recognized. One volcanic episode that produced widespread intercrater plains occurred during the period of the Late Heavy Bombardment and markedly altered the surface in many areas. The second episode is typified by the smooth plains interior and exterior to the Caloris basin, both of which have a different crater size-frequency distribution than the intercrater plains, consistent with a cratering record dominated by a younger population of impactors. These two phases may have overlapped as parts of a continuous period of volcanism during which the volcanic flux tended to decrease with time. The youngest age of smooth plains volcanism cannot yet be determined, but at least small expanses of plains are substantially younger than the plains associated with the Caloris basin. The spatial and temporal variations of volcanic resurfacing events can be used to reconstruct Mercury's geologic history from images and compositional and topographic data to be acquired during the orbital phase of the MESSENGER mission.

1. Introduction

The origin of the objects responsible for the inner solar system cratering record has been debated for decades. In particular, the origin of the Late Heavy Bombardment (LHB) has had a variety of interpretations since it was confirmed during the Apollo era (e.g., Ivanov et al., 2002; Gomes et al., 2005). However, a number of recent studies (e.g., Gomes et al., 2005; Strom et al., 2005) indicate that the impact craters were primarily caused by asteroids and that the period of Late Heavy Bombardment was a cataclysmic event, most likely the result of resonant sweeping of the asteroid belt by the inward migration of Jupiter from about 3.9–3.8 Ga (Gomes et al., 2005). At that time the size distribution of main-belt asteroids was apparently the same as it is today (Bottke et al., 2005). The post-LHB impacts are thought to be dominated by Yarkovsky-effect-driven near-Earth asteroids (Morbidelli and Vokrouhlicky, 2003; Strom et al., 2005). These interpretations are adopted here.

From studies of the crater size-frequency distributions on the Moon and terrestrial planets, it has been recognized that the inner solar system has been dominated by two populations of impacting objects (Strom et al., 2005). The first population (Population 1) is the result of the LHB, and the second population (Population 2) has been mostly derived from near-Earth asteroids. Population 1 craters have a complex size distribution with a -2.2 slope to the differential size-frequency distribution between diameters of about 10 and 65 km. Population 2 craters have a differential size-frequency distribution with a –3 slope. Fig. 1 shows an R plot of the size-frequency distributions for these crater populations on the Moon and Mars.[1] (For more comprehensive sets of plots of

[1] Throughout this paper we display the crater size distributions using the relative plotting method (or R plot) that was devised to better show the size distribution of craters and crater number densities to determine relative ages. The R plot provides a more sensitive and discriminating comparison tool than cumulative distribution plots, which tend to smear out important details of the crater size-frequency distribution curves and can lead to erroneous interpretations. For an R plot, the size distribution is normalized to a power law differential size distribution function, $dN(D) \sim D^p dD$, where D is diameter and $p=-3$, because most crater size distributions are observed to have a slope within ± 1 of -3 on a log-log plot. The equation for R is: $R=D^3N/A(b_2-b_1)$, where D is the geometric

* Corresponding author.
E-mail address: rstrom@lpl.arizona.edu (R.G. Strom).

0032-0633/$ - see front matter © 2011 Elsevier Ltd. All rights reserved.
doi:10.1016/j.pss.2011.03.018

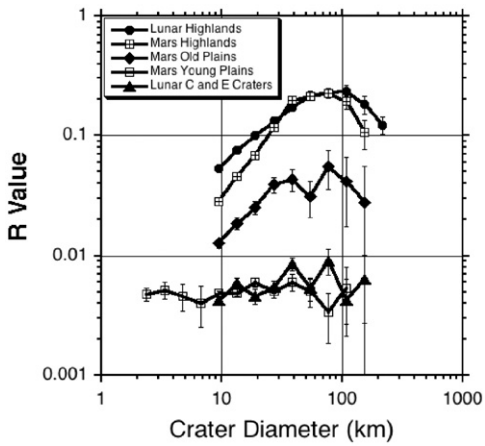

Fig. 1. This R plot shows two crater populations on the Moon and Mars. The lunar highlands, Mars highlands, and Mars old plains are Population 1 craters that represent the period of Late Heavy Bombardment. The post-mare Copernican (C) and Eratosthenian (E) craters represent Population 2 on the Moon. The Mars young plains have the same crater distribution as the lunar Copernican and Eratosthenian craters and are also Population 2. See Strom et al. (2005) for more examples of these two crater populations.

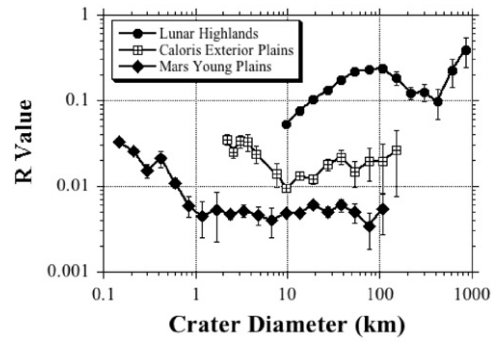

Fig. 2. This R plot shows the large size of secondary impact craters on Mercury compared to those on Mars. The secondaries are represented by the upturn in the curves at smaller diameters. On Mars the upturn begins at diameters less than about 1 km, whereas on Mercury it begins at a diameter of about 10 km. The distribution for the lunar highlands is shown for comparison.

these two populations see Strom et al., 2005). The three top curves (lunar highlands, Mars highlands, and Mars old plains) are dominantly the result of Population 1 craters, whereas the two bottom curves (lunar Corpernican and Eratosthenian craters, and Mars young plains) are the result of Population 2 craters. As discussed later, the difference in impact velocities between Mercury, the Moon, and Mars has resulted in horizontal displacements of the size-frequency distributions of Population 1 crater curves for these objects.

In addition to these two primary impact populations, a third population of craters occurs at relatively small diameters (less than ~1 to 10 km, depending on the target body) and has a fairly steep positive slope on an R plot (Fig. 2). These craters are interpreted to be the secondary impact craters produced by ejecta from large craters and basins (Strom et al., 2008). Many craters of this size range occur in strings or clusters indicative of secondary impact craters. On Mercury, however, a given size crater apparently has larger secondaries than on the Moon and Mars (Fig. 2) (Gault et al., 1975). In particular, on Mercury substantial numbers of secondary craters associated with basins have diameters up to, or greater than, 10 km, affecting the crater size distributions in the 8–11 km size bin and sometimes larger (Strom et al., 2008). On the Moon, secondaries from the Orientale and Imbrium basin can also reach diameters of 10–20 km (Wilhelms et al., 1978), but they are not sufficiently abundant to change the crater size-frequency distribution of the highlands at these diameters. On other terrestrial planets, secondary impact craters begin to dominate the population only at diameters less than about 1 km as shown for Mars in Fig. 2.

The reason for the larger secondaries on Mercury is not well understood. The principal difference in impact parameters from those of other solar system bodies is the much higher impact velocities on Mercury. For example, the mean impact velocity of asteroids at Mercury is 38.1 km/s compared to 18.9 km/s for the Moon and 12.4 km/s for Mars (Minton and Malhotra, 2010). The surface gravity of Mercury is also higher than that on the Moon but about the same as that of Mars. As a result of the higher surface gravity, continuous ejecta blankets for craters on Mercury are more closely concentrated near the crater rim than on the Moon (Gault et al., 1975). Other parameters being equal, the higher impact velocities on Mercury should produce more fragmentation and smaller secondaries (H.J. Melosh, personal communication, 2010) than on other bodies. However, if the target material is much stronger on Mercury than on other bodies, then larger secondaries may be produced. We do not know the strength of the surface material on Mercury, but the heavily cratered terrain on Mercury has been much more affected by volcanic plains formation than the lunar highlands, the surface of which is primarily a megaregolith and probably weaker than volcanic rock. This difference may, at least in part, be responsible for the larger secondaries on Mercury. Another possibility is that the higher gravity causes the ejected fragments to form more concentrated clusters that in turn form larger secondaries. However, more research on the mechanics of impacts into targets of differing strengths and more comparative secondary crater counts on Mercury, the Moon, and Mars are needed before we can fully address this important problem. This paper treats the crater populations only at diameters greater than 8 km so as to minimize, but not necessarily eliminate, the effects of secondary impact craters.

The crater size-frequency distribution on Mercury varies from region to region. The purpose of this paper is to explore the reasons for these variations and the implications for the surface history of the planet. We utilize images collected during the flybys of Mercury by Mariner 10 and by the MErcury Surface, Space ENvironment, GEochemistry, and Ranging (MESSENGER) spacecraft. Four regions along the terminator were selected from the approach side of Mercury for the first MESSENGER flyby, and one on the departure side containing the Raditladi basin was selected for comparison. Three other areas were measured in the terminator region on the departure side of the second MESSENGER flyby. In all cases the lighting conditions were similar and good for topographic discrimination. Furthermore, the resolution of the mosaics from which the areas were selected was similar, and the smallest diameter counted (9 km) was well above the resolution limits. In several cases the individual areas were combined when the size-frequency distributions were similar in each area. In such cases the shapes of the curves were similar

(*footnote continued*)
mean diameter of the size bin, N is the number of craters in the size bin, A is the area over which the counts were made, and b_1 and b_2 are the lower and upper limit of the size bin, respectively. The size bins are usually defined in $\sqrt{2}$ increments because there are many more small craters than large craters. In an R plot, log R is plotted on the ordinate and log D is plotted on the abscissa. A $p=-3$ distribution plots as a horizontal straight line; a $p=-2$ distribution slopes down to the left at an angle of 45°, and a $p=-4$ distribution slopes down to the right at 45°. The vertical position of the line is a measure of crater density; the higher the vertical position, the higher the crater density and older the surface (see Crater Analysis Techniques Working Group, 1978, 1979).

and the curves generally overlapped within two standard deviations. It should be understood that these regions represent a relatively small fraction of the surface area of the planet, but they clearly show regional variations that probably typify much of the planet.

In this paper we argue that for any given region the crater size-frequency distribution at diameters greater than about 8 km depends on the following three factors: (1) the age of the surface, (2) the abundance of plains and the temporal history of their formation, and (3) the proximity to large craters and basins. The formation of both intercrater plains and smooth plains obliterated some fraction of the smaller craters in some regions, steepening the slope on an R plot. This pattern also holds for old surfaces on Mars (see Fig. 1). On Mercury, secondary impact craters can cause the size distribution to shoal and turn upward at diameters <20 km (Strom et al., 2008). On the youngest surfaces the differential size-frequency distribution for primary craters flattens out to an approximate −3 slope, probably representing crater Population 2. The shape and vertical position (relative age) of the crater size-frequency distribution provide insights into the resurfacing history of the planet.

2. Plains and secondary crater modification of the primary crater size-frequency distribution

Mercury experienced widespread volcanism that varied in timing and extent from region to region (Head et al., 2008, 2009; Denevi et al., 2009). This volcanism was primarily manifested in plains formation, although other volcanic landforms are also present. From Mariner 10 images, the plains were divided into two types on the basis of the abundance of superposed craters (Strom et al., 1975). Plains with a higher abundance of both primary and secondary craters were called intercrater plains, and those with a lower abundance and smoother appearance were called smooth plains (Fig. 3). Intercrater plains were interpreted as either basin ejecta (Wilhelms, 1976) or volcanic plains emplaced during the period of LHB (Strom et al., 1975; Strom, 1977). MESSENGER studies indicate that most plains (intercrater and smooth) appear to be primarily volcanic in origin (Head et al., 2008, 2009; Strom et al., 2008; Denevi et al., 2009). The most extensive smooth plains recognized from Mariner 10 observations were within and surrounding the Caloris basin and in a broad area of the north polar region known as Borealis Planitia. Patches of smooth plains were also recognized within heavily cratered terrain. Because of the lower crater abundances on the smooth plains of Borealis Planitia, plains interior to the Tolstoj basin, and plains interior and exterior to the Caloris basin, these units were interpreted on the basis of Mariner 10 images to be younger than intercrater plains (Strom et al., 1975). The Borealis plains were interpreted from Mariner 10 images to lie within a large ancient and degraded impact basin. However, neither the Mariner 10 nor MESSENGER flybys imaged this region well, so characterization of these plains must wait for MESSENGER's orbital mission phase.

From Mariner 10 images, the smooth and intercrater plains were each interpreted as having been emplaced within a short-lived volcanic episode that ceased when Mercury entered a stage of global contraction marked by the formation and continued activity on the great thrust faults associated with the planet's system of lobate scarps (Strom et al., 1975). The horizontal compressive stress in Mercury's lithosphere produced by global contraction was considered to have acted to impede magma from reaching the surface (Solomon, 1978). However, new crater counts on interior plains associated with the young Rachmaninoff peak-ring basin (290 km in diameter) indicate that at least isolated volcanism is younger than previously recognized (Prockter et al., 2010).

Plains resurfacing markedly affected the cratering record in a variety of ways. In many areas, the crater distribution on Mercury follows at a more or less uniformly lower crater density than the lunar highlands at crater diameters less than about 100 km. However, in other areas the crater density follows that of the lunar highlands for craters with diameters larger than 20 km, but the obliteration of smaller craters has steepened the curve at smaller diameters. These differences in crater distributions from those of the lunar highlands are both probably a consequence of the burial of craters by intercrater and smooth plains. The amount of crater obliteration and the diameter of onset depend on the thicknesses and, therefore, volumes of both intercrater and smooth plains, their distribution in the area counted, and the ages of the plains units (for example, see Fig. 9 in Head et al., 2009).

Examples of these generalities are evident in the areas shown in Fig. 4, which are near the terminator on the approach hemisphere of MESSENGER's first flyby (M1). Four areas on the image were counted, but because the counts on Areas 1 and 2 were similar to each other, as were the counts on Areas 3 and 4, two larger regions were created by combining each of the pairs of areas to improve the statistics. The combined areas counted are labeled as Areas 1 and 2 and Areas 3 and 4 as shown in Fig. 4. Areas 1 and 2 are heavily cratered with plains interspersed between clusters of craters. Areas 3 and 4 include a greater abundance of plains. The western portion of these areas is also crossed by strings of large secondary craters from the Beethoven basin, the rim of which is shown in Fig. 4.

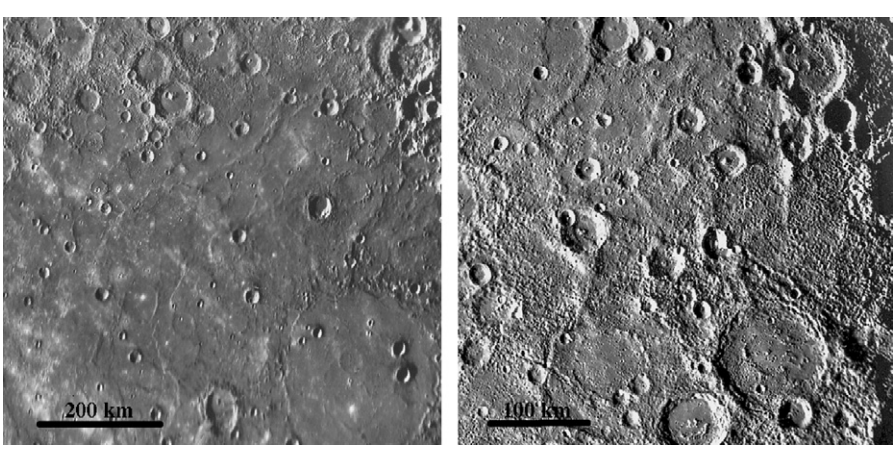

Fig. 3. These two Mariner 10 images show smooth plains in the Borealis Planitia region (left) and intercrater plains in the south polar region of Mercury (right). The older intercrater plains have a higher density of primary and secondary craters.

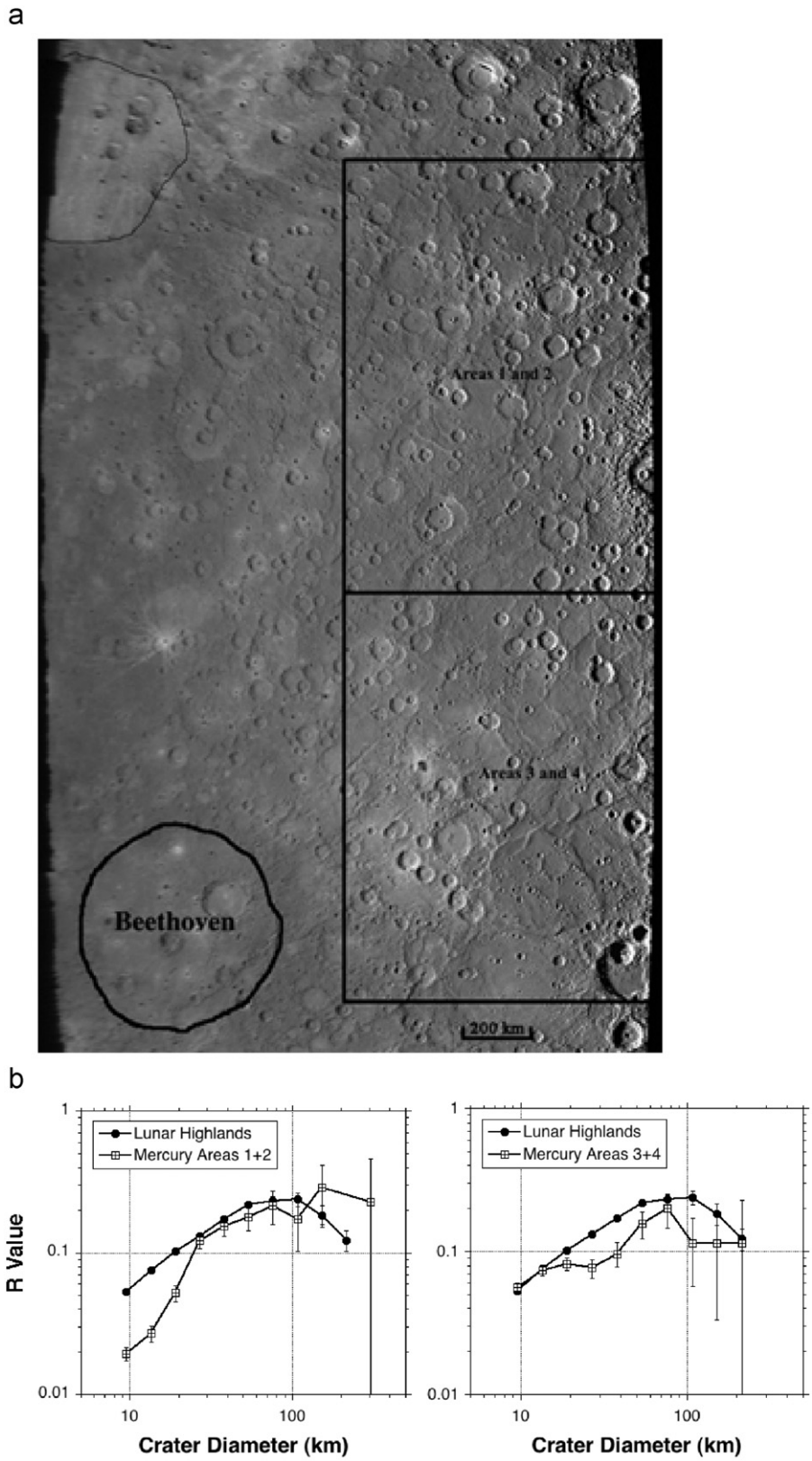

Fig. 4. (a) MESSENGER mosaic of the approaching face of Mercury during the first flyby, showing Areas 1–4, for which crater counts are reported here. Both smooth and intercrater plains formation, as well as secondary craters from the Beethoven basin and a candidate older basin outlined at upper left, likely contributed to the crater distributions shown in (b). (b) R plots of the crater size distribution in Areas 1 and 2 (left) and Areas 3 and 4 (right) compared to that of the lunar highlands. The steeper part of the curve at diameters less than about 30 km in Areas 1 and 2 (left) is probably due to obliteration of craters by plains formation. The lower overall crater density and upturn in the curve at smaller diameters in Areas 3 and 4 (right) are probably due to plains formation and secondaries from Beethoven. See the text for further explanation.

Two R plots of the combined areas are compared to that of the lunar highlands in Fig. 4b. At crater diameter D between about 25 and 100 km, the crater size-frequency distribution for Areas 1 and 2 (Fig. 4b, left) is very similar in shape and crater density to that of the lunar highlands. However, at diameters less than about 25 km, Areas 1 and 2 have fewer craters than the lunar highlands. The difference ranges from 54 craters in the 16–22 km size bin to 154 craters in the 8–11 km size bin, with a total difference of over 300 craters. These differences are interpreted primarily as the result of plains emplacement. The fact that most of the crater distribution nearly follows the curve for the lunar highlands of $D > 25$ km suggests that plains emplacement occurred after or very near the end of LHB, by which time many of the larger craters on older surfaces of Mercury and the Moon would have formed. Also, there is little or no flattening of the curve in the 10 km size bin due to secondaries (see below), again suggesting that plains emplacement was at a time when the formation of large impact craters was relatively rare, i.e., younger than the LHB.

The crater size-frequency distribution for Areas 3 and 4 (Fig. 4b, right) differs from that of Areas 1 and 2. It generally has a lower crater density than the lunar highlands. However, it levels out at diameters less than about 30 km, matches the lunar highlands curve at about 15 km diameter, and then follows it downward with decrease in diameter to $D \sim 8$ km. The reason that the distribution flattens out rather than continuing to rise up may be due to a later and more local volcanic episode that destroyed the smaller secondaries. We infer that the plains formation in this area apparently reset the surface during the period of the LHB. There is a small region of smooth plains at the southern end of Areas 3 and 4 that probably represents a later volcanic episode. However, smooth plains do not cover a large fraction of the area and do not markedly influence the crater size-frequency distribution. The Beethoven basin-forming impact produced large secondary craters in the area and modified the crater curve below 30 km diameter.

In most regions of Mercury the crater size-frequency distribution has been affected by secondary impact craters at diameters less than about 10–15 km. These secondaries cause a flattening or upturn in the R plot at diameters between about 8 and 11 km. The diameter at which this occurs depends on the proximity to relatively large fresh basins over about 200 km in diameter, as occurs near Areas 3 and 4 (Fig. 4a).

A heavily cratered area of Mercury in the vicinity of the 260-km-diameter Raditladi peak-ring basin, imaged on the departing hemisphere during MESSENGER's first flyby, is shown in Fig. 5a. The crater size-frequency distribution for that area, shown in Fig. 5b is similar in shape to that of the lunar highlands but less cratered at diameters between about 20 and 100 km. The flattening and upturn at diameters less than 20 km is primarily due to secondary craters from the Raditladi basin (the largest crater shown on the R plot in Fig. 5b). Most of the secondaries are less than 20 km diameter, and they primarily affect counts in size bins corresponding to diameters less than 8–10 km.

A heavily cratered area in the departure mosaic from MESSENGER's second flyby (M2) is shown in Fig. 6a. The region, divided into three counting areas, is a mixture of craters and plains. There are several large craters with numerous associated secondaries. Each of the areas shown in Fig. 6a has similar crater size distributions, so they were combined for better statistics.

An R plot of the outlined regions in Fig. 6a is shown in Fig. 6b. Compared to the lunar highlands, the crater density is significantly and uniformly lower at diameters less than about 150 km. This pattern suggests that the area had a major resurfacing event that obliterated most craters with diameters less than about 120 km. That event was followed by an episode of cratering dominated by Population 1 objects forming its current crater density. This major resurfacing event must have occurred during the period of the LHB, because the resurfaced area preserves a high density of Population 1 craters. The curve is slightly steeper than the lunar curve at diameters less than about 30 km, suggesting that the plains in the western region have buried a portion of the craters at lesser diameters. These plains are probably relatively young, because they have obliterated secondaries from the relatively fresh crater marked "A." The upturn in the distribution at about 10 km diameter is due to secondaries from the largest craters in the eastern part of the region. These secondaries can be seen in Fig. 6a as clusters and chains radial to several of the largest craters. This upturn was first recognized in the Mariner 10 crater counts and was also interpreted due to secondaries (Strom et al., 1975; Strom, 1977).

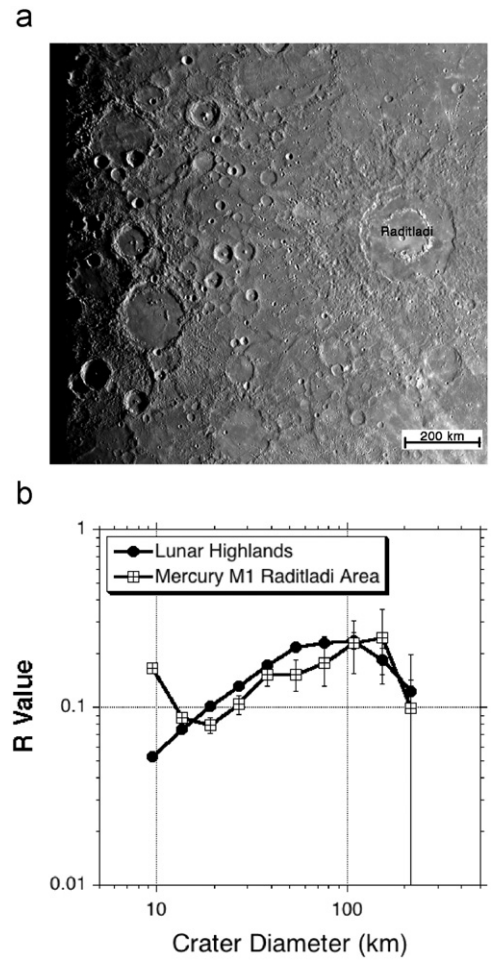

Fig. 5. (a) Areas for which craters were counted to produce the R plot is shown in (b). Numerous secondaries from the 260-km-diameter Raditladi basin and other large craters have greatly affected the crater curve. This image is of a portion of Mercury's departing hemisphere during MESSENGER's first flyby. (b) R plot of the crater size-frequency distribution for the area shown in (a) compared to that for the lunar highlands. The Mercury curve is slightly below that of the lunar highlands at diameters less than about 100 km. The flattening and upturn of the curve at diameters less than 20 km is due to secondaries from the Raditladi impact and other large craters.

3. The general cratering record

To generalize the cratering record in heavily cratered areas on Mercury, Fig. 7 shows an R plot for which counting statistics have been combined for nine areas, eight areas of heavily cratered terrain imaged during M1 and M2 plus counts in heavily cratered

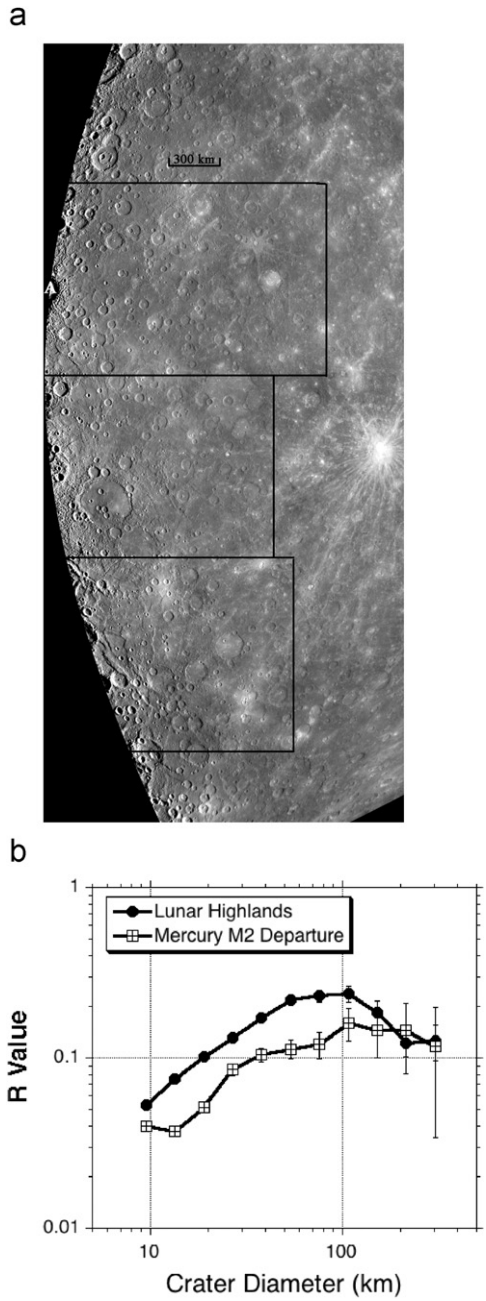

Fig. 6. (a) Region from the M2 departure mosaic within which the crater counts depicted in (b) were made. The three areas shown were counted separately, but the size distributions were so similar that they were combined for better statistics. (b) R plot of the crater size-frequency distribution in the three areas of the M2 departure mosaic shown in (a). The plot is compared to that for the lunar highlands. At diameters less than about 150 km the curve is systematically below the distribution for the lunar highlands, indicating a major resurfacing event during the period of Late Heavy Bombardment. The upturn at 10 km is due to secondary craters from the largest craters in the area. See the text for further explanation.

terrain imaged by Mariner 10. There is no overlap between the Mariner 10 and MESSENGER counting areas. The resulting distribution shows that when regions depleted of craters by plains formation are combined with areas containing many large secondary craters and other more uniformly cratered regions at higher crater densities, the resulting curve is very similar in shape to that for the lunar highlands but with a lower overall density at diameters less than 100 km. At the smallest diameter ($\sim$10 km), however, the size-frequency distribution of Mercury's heavily cratered terrain turns upward, showing the signature of

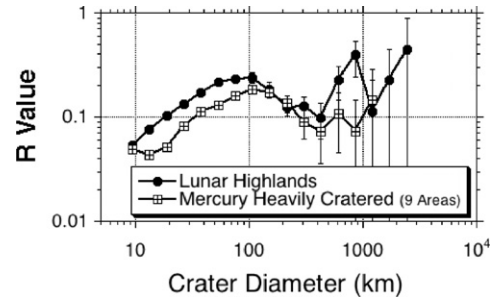

Fig. 7. R plot of the crater size-frequency distribution for a total of nine regions of heavily cratered terrain on Mercury (eight from MESSENGER images and one from Mariner 10 images) compared to the distribution for the lunar highlands. At diameters below 100 km the distribution for Mercury heavily cratered terrain is systematically lower than that for the lunar highlands except for the upturn at diameters less than 10 km due to secondaries. See the text for further explanation.

secondaries that are so ubiquitous that their influence on the distribution is apparent even when averages are made over a large area of the planet. At diameters greater than about 100 km the shape and crater density of the distribution for Mercury's heavily cratered terrain is very similar to that of the lunar highlands. Variations in the crater size-frequency distribution from area to area due to plains formation and secondaries shows that on Mercury it is necessary to examine relatively local areas if the resurfacing history and inferred regional geologic history are to be reconstructed reliably.

Because of the better statistics at larger diameters for which modification by plains is minimal, Fig. 7 shows that the large-crater downturn in the Mercury crater size-frequency distribution occurs at a larger diameter bin than for the Moon. On Mars, the downturn occurs at an even smaller diameter bin than for the Moon (see Fig. 1). On the Moon this downturn starts at about the 107 km bin, but on Mars it starts at about the 76 km bin, and on Mercury at about the 152 km bin. These differences are consistent with an origin of the impactors from the main asteroid belt, because the impact velocities of these objects are much higher on Mercury (median velocity 38.1 km/sec) and much lower on Mars (median velocity 12.4 km/sec) than on the Moon (median velocity 18.9 km/sec) (Minton and Malhotra, 2010). For this explanation to hold, the diameter at which the distribution downturn occurs should correspond to a similar projectile size on each body. From the Pi Scaling law (Holsapple and Schmidt, 1987; Collins et al., 2005), the projectile size at these downturn diameters are indeed similar: 4.7 km diameter for the Moon, 4.4 km for Mars, and 4.9 km diameter for Mercury. For comparison, if there were no offsets and the downturns began at 107 km for all three bodies, the projectile sizes would be 6.2 km diameter on Mars and 3.3 km diameter on Mercury compared to 4.2 km for the Moon. The different diameters at downturn are therefore consistent with the hypothesis that the objects responsible for Late Heavy Bombardment originated from main-belt asteroids. These shifts, and their implications for the orbits of the impacting objects, were first described by Strom and Neukum (1988).

4. Age and the primary crater population

It was known from Mariner 10 observations that Population 1 craters dominated the cratering record on Mercury (Strom et al., 1975; Strom and Neukum, 1988), but not enough younger smooth plains were counted to determine if Population 2 craters were present. MESSENGER's first flyby combined with Mariner 10 terminator coverage of eastern Caloris provides sufficient coverage of the large expanses of smooth plains interior and exterior to

the Caloris basin to make this assessment. Crater counts on these plains show that they are dominated by Population 2 craters (Strom et al., 2008). As shown in Fig. 8, R plots are compared for the Caloris Montes (part of the dissected rim of the Caloris basin), Caloris exterior plains, and Mercury heavily cratered terrain. Power laws have been fit to each distribution. Both the heavily cratered terrain and the Caloris rim deposits have the same crater size-frequency distribution, but the Caloris Montes are at a low crater density. Although the Caloris rim statistics have rather large error bars, it appears that the Caloris impact was part of the LHB that occurred during the main bombardment of the inner solar system. In contrast, the plains exterior and interior to Caloris were emplaced near the end of the LHB because they have a lower crater density and their crater size-frequency distributions have a shape consistent with mostly Population 2 craters.

The fraction of Population 1 and Population 2 craters on the Caloris plains may be estimated by modifying the lunar highlands (Population 1) differential size-frequency distribution between diameters 10 and 100 km (-2.2 slope) with varying percentages of the Population 2 curve differential size-frequency distribution (-3 slope). This was done after the best-preserved (so-called Class 1, Arthur et al., 1963) craters (Population 2) had been subtracted from the highlands curve. Fig. 9 shows the size-frequency distribution of the Caloris interior plains (left) and exterior plains (right) compared to best-fitting mixtures of Population 1 and Population 2 craters. The slightly lower crater density of the exterior plains indicates that, on average, they are younger than the interior plains (Strom et al., 2008). This age difference is consistent with the shallower slope of the curve for exterior plains. Although the error bars are relatively large, the fits indicate that Population 2 dominates the Caloris plains crater population by about 9 to 1 over Population 1. If these plains were emplaced over a narrow time interval, the results shown in Fig. 9 suggest that volcanic flooding of the Caloris interior and exterior occurred very near to the end of Late Heavy Bombardment, or about 3.8 Ga (Strom et al., 2008). Alternatively, flooding may have been initiated near the end of LHB but continued thereafter for an undetermined interval as long as some fraction of the oldest surfaces was preserved against burial by younger flows.

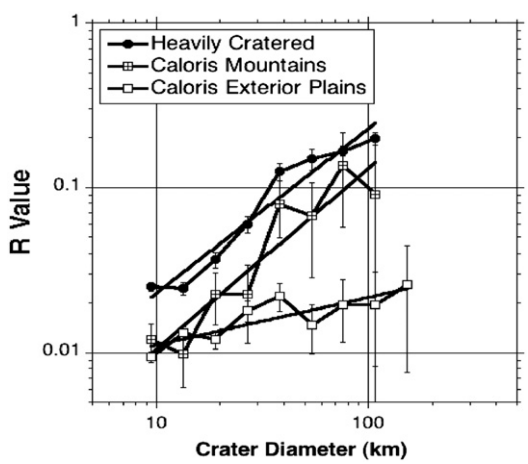

Fig. 8. R plots for Mercury heavily cratered terrain, Caloris Montes rim material, and the Caloris exterior plains. For each curve a power-law fit is shown by a bold straight line. The Mercury heavily cratered terrain and Caloris rim material have the same crater population (Population 1) but the Caloris exterior (and interior) plains have a lower crater density and a different crater population (Population 2). See the text for further explanation.

5. Conclusion

We interpret the impact cratering record on Mercury to show two primary crater populations similar to those seen on the Moon and Mars. However, the crater size-frequency distribution on Mercury shows pronounced regional variations that we argue are primarily the consequence of differences in the extent and age of volcanic plains emplacement. Also, the formation of large craters and basins has produced large secondaries that have affected the size distribution at diameters less than about 10–20 km. In some areas plains formation has obliterated a substantial number of craters to steepen the crater curve at smaller diameters. In other areas, almost the entire curve has been lowered as a consequence of extensive volcanism that resurfaced the region during the period of the Late Heavy Bombardment. This volcanism was followed by re-cratering that raised the crater curve, but to a lower density than for unaffected areas. There are variations between these two types of resurfacing indicating a rather complicated history of volcanic plains formation. The age of the youngest resurfacing is not yet known, but it could be considerably younger than the Caloris plains, at least a portion of which were emplaced near the end of Late Heavy Bombardment. Young volcanism associated with the relatively recent Rachmaninoff basin (Prockter et al., 2010) suggests that at least some of the plains may span a considerable range of ages.

The orbital phase of the MESSENGER mission will provide an opportunity to determine the resurfacing history of Mercury on a global scale from variations of the cratering record. In combination with geologic mapping and the determination of compositional and topographic variations, additional studies along the lines described in this paper should enable considerable progress to be made towards understanding the geological evolution of Mercury.

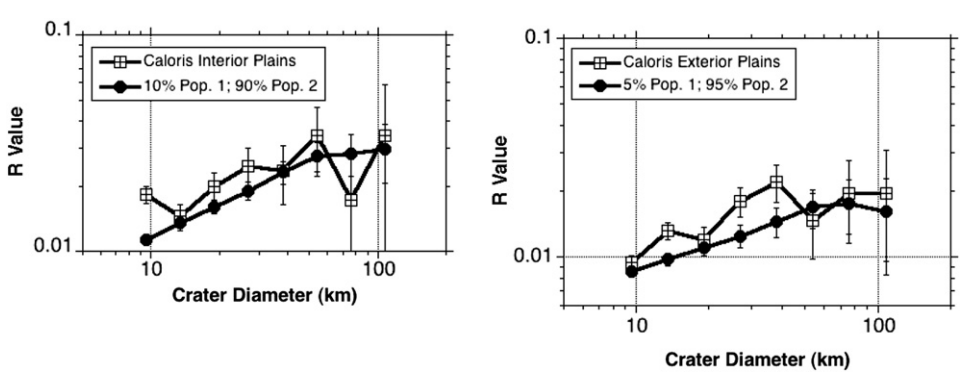

Fig. 9. R plots of the Caloris interior (left) and exterior (right) plains compared to mixtures of Population 1 and Population 2 craters with 10% and 5% contributions from Population 1, respectively. The error in this comparison is about $\pm 5\%$. The interior and exterior Caloris plains are dominated by Population 2 craters. See the text for further explanation.

References

Arthur, D.W.G., Agnieray, A.P., Horvath, R.A., Wood, C.A., Chapman, C.R., 1963. The system of lunar craters, quadrant I. Comm. Lunar Planet. Lab 2, 71–78.

Bottke, W.F., Durda, D.D., Nesvorny, D., Jedicke, R., Morbidelli, A., Vokrouhlicky, D., Levison, H., 2005. The fossilized size distribution of the main asteroid belt. Icarus 175, 111–140.

Collins, G.S., Melosh, H.J., Marcus, R.A., 2005. Earth impact effects program: a web-based computer program for calculating the regional environmental consequences of a meteoroid impact on Earth. Meteorit. Planet. Sci 40, 817–840.

Crater Analysis Techniques Working Group, 1978. Standard Techniques for Presentation and Analysis of Crater Size-Frequency Data. Technical Memorandum 79730, NASA, Washington, DC, 20 pp.

Crater Analysis Techniques Working Group, 1979. Standard analysis techniques for presentation and analysis of crater size-frequency data. Icarus 37, 467–474.

Denevi, B.W., Robinson, M.S., Solomon, S.C., Murchie, S.L., Blewett, D.T., Domingue, D.L., McCoy, T.J., Ernst, C.M., Head, J.W., Watters, T.R., Chabot, N.L., 2009. The evolution of Mercury's crust: a global perspective from MESSENGER. Science 324, 613–618.

Gault, D.E., Guest, J.E., Murray, J.B., Dzurisin, D., Malin, M.C., 1975. Some comparisons of impact craters on Mercury and the Moon. J. Geophys. Res. 80, 2444–2460.

Gomes, R., Levison, H.F., Tsiganis, K., Morbidelli, A., 2005. Origin of the cataclysmic Late Heavy Bombardment period of the terrestrial planets. Nature 435, 466–469.

Head, J.W., Murchie, S.L., Prockter, L.M., Robinson, M.S., Solomon, S.C., Strom, R.G., Chapman, C.R., Watters, T.R., McClintock, W.E., Blewett, D.T., Gillis-Davis, J.J., 2008. Volcanism on Mercury: evidence from the first MESSENGER flyby. Science 321, 69–72.

Head, J.W., Murchie, S.L., Prockter, L.M., Solomon, S.C., Chapman, C.R., Strom, R.G., Watters, T.R., Blewett, D.T., Gillis-Davis, J.J., Fassett, C.I., Dickson, J.L., Morgan, G.A., Kerber, L., 2009. Volcanism on Mercury: evidence for extrusive and explosive activity and the volcanic origin of plains. Earth Planet. Sci. Lett. 285, 227–242.

Holsapple, K.R., Schmidt, R.M., 1987. Point-source solution and coupling parameters in cratering mechanics. J. Geophys. Res. 92, 6350–6376.

Ivanov, B.A., Neukum, G., Bottke, W.F., Hartman, W.K., 2002. The comparison of size-frequency distributions of impact craters and asteroids and the planetary cratering rate. In: Bottke, W.F., Cellino, A., Paolicchi, P., Binzel, R.P. (Eds.), Asteroids III. University of Arizona Press, Tucson, Ariz., pp. 89–101.

Minton, D.A., Malhotra, R., 2010. Dynamical erosion of the asteroid belt and implication for large impacts in the inner solar system. Icarus 207, 744–757.

Morbidelli, A., Vokrouhlicky, D., 2003. The Yarkovsky-driven origin of near-Earth asteroids. Icarus 163, 120–134.

Prockter, L.M., Ernst, C.M., Denevi, B.W., Chapman, C.R., Head, J.W., Fassett, C.I., Merline, W.J., Solomon, S.C., Watters, T.R., Strom, R.G., Cremonese, G., Marchi, S., Massironi, M., 2010. Evidence for young volcanism on Mercury from the third MESSENGER flyby. Science 329, 668–671.

Solomon, S.C., 1978. On volcanism and thermal tectonics on one-plate planets. Geophys. Res. Lett. 5, 461–464.

Strom, R.G., 1977. Origin and relative age of lunar and mercurian intercrater plains. Phys. Earth Planet. Inter. 15, 156–172.

Strom, R.G., Trask, N.J., Guest, J.E., 1975. Tectonism and volcanism on Mercury. J. Geophys. Res. 80, 2478–2507.

Strom, R.G., Neukum, G., 1988. The cratering record on Mercury and the origin of impacting objects. In: Vilas, F., Chapman, C.R., Matthews, M.S. (Eds.), Mercury. University of Arizona Press, Tucson, Ariz., pp. 336–373.

Strom, R.G., Malhotra, R., Ito, T., Yoshida, F., Kring, D.A., 2005. The origin of planetary impactors in the inner solar system. Science 309, 1847–1850.

Strom, R.G., Chapman, C.R., Merline, W.J., Solomon, S.C., Head, J.W., 2008. Mercury cratering record viewed from MESSENGER's first flyby. Science 321, 79–81.

Wilhelms, D.E., 1976. Mercurian volcanism questioned. Icarus 28, 551–558.

Wilhelms, D.E., Oberbeck, V.R., Aggarwal, H.R., 1978. Size-frequency distributions of primary and secondary lunar impact craters. Proc. Lunar Planet. Sci. Conf. 9, 3735–3762.